

# Bacterial Adhesion and Transport in Porous Media: Role of the Secondary Energy Minimum

JEREMY A. REDMAN,  
SHARON L. WALKER, AND  
MENACHEM ELIMELECH\*

Department of Chemical Engineering, Environmental  
Engineering Program, Yale University, P.O. Box 208286,  
New Haven, Connecticut 06520-8286

The adhesion of a well-characterized *Escherichia coli* bacterial strain to quartz sediment grains in the presence of repulsive electrostatic interactions is systematically examined. An increase in the ionic strength of the pore fluid results in an increase in bacterial attachment, despite DLVO calculations indicating a sizable electrostatic energy barrier to deposition. Bacterial deposition is likely occurring in the secondary energy minimum, which DLVO calculations indicate increases in depth with ionic strength. A decrease in the ionic strength of the pore fluid—thereby eliminating the secondary energy minimum—resulted in release of the majority of previously deposited bacteria, suggesting that these cells were deposited reversibly in the secondary minimum. Additionally, bacterial attachment to a quartz surface in a radial stagnation point flow system was absent at ionic strengths less than 0.01 M and resulted in attachment efficiencies over an order of magnitude lower than in the packed-bed column experiments at higher ionic strengths. Because of the hydrodynamics in the radial stagnation point flow system, this observation supports our conclusion that the majority of bacterial deposition in the packed bed occurs in a secondary energy minimum.

## Introduction

Bacterial adhesion to solid surfaces is an important aspect in a number of disciplines, ranging from the development of biomedical materials to water quality control technologies. With regard to subsurface environments, understanding the processes controlling bacterial adhesion and transport is critical. For example, in situ bioremediation efforts often rely on bacterial strains that have low adhesion and enhanced transport (1). A mechanistic understanding of bacterial adhesion will also lead to greater insight into natural filtration of pathogenic microorganisms in groundwater (2).

The physical and chemical factors governing the transport and adhesion of bacteria in aquatic systems have been studied extensively in the past two decades. The factors investigated included cell type (3, 4), hydrophobic interactions (4–6), motility (7, 8), surface charge characteristics (6, 9), and surface features (e.g., lipopolysaccharides, fimbriae) (10–12). Despite these efforts, the mechanisms governing the adhesion of bacterial cells onto sediment grains are not fully understood.

Under controlled laboratory conditions, the initial adhesion of bacterial cells onto solid surfaces in aquatic systems is generally thought to be similar to that of depositing colloidal particles. For such cases, classic Derjaguin–Landau–Verwey–Overbeek (DLVO) theory has been applied to explain this attachment behavior (7, 11, 13–19). Specifically, DLVO theory states that the interactions between a colloidal particle and a collector surface can be expressed as the sum of the attractive van der Waals and electrostatic double layer interactions, which can be either attractive or repulsive. In some cases, attempts have been made to reconcile discrepancies between DLVO predictions and observations by including non-DLVO forces, such as Lewis acid–base interactions, into the so-called extended DLVO calculations (11, 12, 15, 20, 21).

In many natural and engineered systems, both the bacterial cells and the collector surfaces have negative surface potentials, giving rise to repulsive electrostatic interactions on close approach. Under such conditions, bacteria are frequently observed to deposit, despite DLVO predictions to the contrary (11, 19). For example, Truesdail et al. (17) found attachment of several different bacterial strains to Ottawa sand, in the presence of calculated energy barriers ranging up to 1000 kT. This observation was attributed to bacterial deposition onto local surface charge heterogeneities on the sand grains, which are not accounted for by classical DLVO theory. In a study utilizing a parallel plate deposition system, Meinders et al. (21) observed a similar behavior, where several bacterial strains attached to glass surfaces despite the very large calculated energy barriers. Meinders et al. postulated that bacterial deposition occurred in the secondary energy minimum, based on a correlation between the deposition rate and the calculated secondary minimum depth.

The studies discussed previously were unsuccessful in quantitatively describing bacterial adhesion with DLVO theory. Moreover, many of these investigations used columns packed with sand (21) or soda-lime glass beads (10, 16, 19). While these collector grains may be uniform in size, they exhibit chemical heterogeneities that have been shown to influence deposition behavior (22). Similarly, studies examining bacterial adhesion in other experimental systems, such as parallel plate and stagnation point flow chambers, often use glass surfaces that also contain chemical heterogeneities (21). These heterogeneities provide locally favorable regions in which bacteria can adhere in a primary energy minimum, which otherwise cannot be predicted by classical DLVO theory that assumes a uniform surface charge of collector surfaces.

In this study, the transport and deposition kinetics of a well-characterized *Escherichia coli* strain under repulsive electrostatic conditions are systematically investigated. Emphasis is placed on the role of electrostatic double layer interactions in the initial adhesion of bacteria to sediment grains and on whether the observed deposition behavior can be explained by classical DLVO theory. To minimize charge heterogeneity effects, highly cleaned, ultrapure quartz grains were selected as the porous media. In addition to the packed-bed column experiments, we also use a well-characterized experimental system, a radial stagnation point flow cell, where individual bacteria are visualized as they deposit onto a uniformly charged, flat quartz surface. Analysis of the results from these two deposition systems suggests that the secondary minimum plays an important role in the adhesion of bacterial cells to sediment grains in flow through porous media.

\* Corresponding author phone: (203)432-2789; fax: (203)432-2881; e-mail: menachem.elimelech@yale.edu.

## Materials and Methods

**Bacterial Cell Preparation and Growth.** The mutant of the *E. coli* K12 strain, D21, used in this study was obtained from the *E. coli* Genetic Stock Center at Yale University. To visualize the cells in the radial stagnation point flow system, a plasmid coding for an enhanced green fluorescing protein and gentamicin resistance (23) was introduced to the native D21 cell by electroporation (24). The resulting transformed D21 cell line is referred to as D21g. Cells were grown in Luria–Bertani broth (LB broth, Fisher, Fair Lawn, NJ) at 37 °C in the presence of 0.03 mg/L gentamicin (Sigma, St. Louis, MO) until reaching mid-exponential phase (3 h), at which time they were harvested for use. Exponential-phase cells were pelleted by centrifugation (Sorvall RC26 Plus Centrifuge) for 15 min at 3823g in a SS34 rotor (Kendro Laboratory Products, Newtown, CT). The growth medium was decanted, and the pellet was resuspended in a KCl electrolyte solution. The cells were pelleted and rinsed with fresh electrolyte solution in this manner two additional times to remove any trace of the growth medium. Electrolyte solutions were prepared with deionized water (Barnstead Thermolyne Corporation, Dubuque, IA) and reagent-grade KCl (Fisher) with no pH adjustment (pH 5.6–5.8).

**Bacterial Cell Size Determination.** An inverted fluorescent microscope (Axiovert 200m, Zeiss, Thornwood, NY) operating in phase contrast mode and connected to a computer was used to take images of the D21g cells suspended in electrolyte solution (approximately  $10^7$  cells/mL in 10 mM KCl). The images were imported into an image processing program (ImageJ, NIH) and analyzed using the built-in routines. The average major and minor axes of the D21g cells were determined to be  $3.7 \pm 1.2 \mu\text{m}$  ( $\pm 1$  standard deviation) and  $1.2 \pm 0.2 \mu\text{m}$  in length, which corresponds to an equivalent spherical diameter of  $1.7 \mu\text{m}$ .

**Granular Porous Media.** Ultrapure quartz sand (Unimin Corporation, Spruce Pine, NC) was used as the packing material for column experiments. The sand was size-fractionated with nylon sieves (U.S. standard size 60 and 100 and 250 and  $150 \mu\text{m}$  openings, respectively). Prior to use, the sand was cleaned thoroughly to remove metal and organic impurities (22, 25). The cleaning steps included soaking the sand in 12 N HCl (Fisher) for at least 24 h, washing in deionized water (Barnstead), and baking the sand at 800 °C for 8 h minimum. Cleaned sand was stored under a vacuum and rehydrated by boiling in deionized water for 1 h prior to packing in the column. Microscopic examination of the quartz sand revealed the grains to be irregular in shape. Sieve analysis resulted in an average grain diameter ( $d_{50}$ ) of  $205 \mu\text{m}$  and a coefficient of uniformity ( $d_{60}/d_{10}$ ) of 1.26. For transport experiments under favorable (nonrepulsive) electrostatic conditions, the quartz was silanized by suspension in a 1% (vol/vol) solution of 3-aminopropyl-triethoxysilane (Sigma) for 5 min, followed by thorough rinsing in deionized water and curing at 80 °C for 24 h (26).

**Quartz Cover Slip.** Round quartz cover slips with a 25 mm diameter and 0.1 mm thickness (Electron Microscopy Sciences, Ft. Washington, PA) were cleaned by soaking initially in a 2% Extran MA02 solution (EM Science, Gibbstown, NJ), followed by a thorough rinsing with ethanol (Pharmco Products, Inc. Brookfield, CT) and deionized water. Cover slips were next sonicated for 10–15 min while submerged in a 2% RBS 35 detergent solution (Pierce, Rockford, IL) followed by a second rinsing with ethanol and deionized water (27). The coverslips were soaked overnight in NOCHROMIX solution (Godax Laboratories, Inc., Takoma Park, MD). After removal from NOCHROMIX solution and rinsing with deionized water, cover slips were mounted in the glass flow cell used in the radial stagnation point flow system as described next. For experiments under favorable

electrostatic conditions, the slides were chemically modified with aminosilane. One side of the quartz cover slip was exposed to a 0.2% (vol/vol) mixture of (aminoethylaminomethyl)-phenethyltrimethoxysilane (Gelest, Inc. Tullytown, PA) in ethanol for 3–5 min at room temperature and then cured for 90 min at 130 °C. The slide was then rinsed with deionized water and installed in the radial stagnation point flow cell.

**Electrokinetic Characterization of Bacterial Cells.** The electrophoretic mobility of the bacterial cells was determined immediately prior to a column transport experiment by diluting the rinsed stock cell suspension into a KCl electrolyte solution at a final concentration between  $10^5$  and  $10^6$  cells/mL. Electrophoretic mobility measurements were conducted at 25 °C using a ZetaPALS analyzer (Brookhaven Instruments Corporation, Holtsville, NY) and were repeated between two and eight times at each ionic strength using freshly rinsed cells. Electrophoretic mobilities were converted to zeta potentials using tabulated numerical calculations of Ottewill and Shaw (28).

**Electrokinetic Characterization of Porous Media.** The electrokinetic properties of the quartz grains were determined by a streaming potential analyzer (EKA, Brookhaven Instruments Corporation). Measurements were conducted by packing a cylindrical cell with quartz grains to a bed depth of 3 cm and then extensively rinsing with deionized water (1 L) followed by electrolyte solution (0.5 L), and finally the sample was equilibrated with fresh electrolyte solution (0.5 L) for 10 min (29). A range of ionic strengths, from 1 to 100 mM KCl, at an unadjusted pH and room temperature was examined. Measurements above 100 mM KCl were not conducted as they exceed the limitation of the instrument. The zeta potential was calculated from the measured streaming potentials as described elsewhere (29).

**Packed-Bed Column Experiments.** Bacterial transport experiments were conducted in glass chromatography columns packed with clean quartz grains. Adjustable bed height columns (Omnifit USA, Toms River, NJ) with a 1 cm inner diameter were used. The columns were wet-packed by allowing the quartz grains to settle in deionized water while the column was agitated. Column packing porosity for this method was determined gravimetrically to be 0.43. The packed columns were equilibrated by sequentially pumping (Model 200 syringe pump, KD Scientific Inc., New Hope, PA) 10 pore volumes of deionized water followed by 10 pore volumes of the background electrolyte solution through the column immediately prior to each experiment. The ionic strength of the pore fluid ranged from 1 to 300 mM and was adjusted through the addition of KCl. A typical experiment involved pumping bacterial cells suspended in an electrolyte solution ( $10^7$ – $10^8$  cells/mL) through the column for 15 min (approximately 4 pore volumes) followed by a bacteria-free solution of the same electrolyte composition for at least 45 min (approximately 12 pore volumes). The approach (superficial) velocity during the column experiments was  $0.021 \text{ cm/s}$ .

In selected experiments, an additional pulse of a bacteria-free low ionic strength solution (0.1 mM KCl) was then applied to the column to examine release of previously deposited bacteria. The fraction of eluted bacteria is defined as the ratio of the amount of eluted cells to amount of deposited cells. The amount of deposited cells was determined by taking the difference between the total amount injected into the column and the numerically integrated amount in the effluent during the breakthrough curve. The amount of bacteria released from the column was determined by numerically integrating over all pore volumes from the time of the elution solution injection until the cell concentration had decayed to background levels.

In all experiments, the bacterial cell concentration in the column effluent was monitored at 2 s intervals by measuring

the absorbance at 280 nm with a UV/vis spectrophotometer (Hewlett-Packard Model 8453) and a 1 cm flow-through cell. After each experiment (ca. 1–1.5 h), the syringes containing bacterial cell solution were briefly shaken and connected directly to the flow-through cell for determination of the influent concentration. The length of the packed beds and cell influent concentrations were adjusted between experiments to obtain absorbance readings that were within the detection range of the spectrophotometer. All solutions had an unadjusted pH between 5.6 and 5.8 at room temperature (22 °C).

**Radial Stagnation Point Flow System.** To further elucidate bacterial adhesion mechanisms, bacterial deposition experiments were conducted in a radial stagnation point flow (RSPF) system. This system consisted of a specially blown glass flow chamber installed on the stage of an inverted fluorescent microscope (Axiovert 200m, Zeiss, Thornwood, NY). The bacterial suspension entered the radially symmetric flow cell through a capillary tube (1 mm inner diameter) oriented in a downward direction. Flow impinged upon a microscope cover glass 2 mm below the capillary opening and traveled radially along the cover slide, exiting the RSPF chamber through a separate capillary tube. An LD Achroplan 40x objective (1.8 mm working distance) located beneath the flow cell was focused on the inner surface of the quartz cover slip. The fluorescent cells were imaged using a fluorescent filter set with an excitation wavelength of 480 nm and emission wavelength of 510 nm (Chroma Technology Corp, Brattleboro, VT). Deposition of bacterial cells was recorded with a digital camera (AxioCam MR monochrome, Zeiss) acquiring images every 20 s over the course of a 20 min injection and analyzed with the supplied software (AxioVision 3.1, Zeiss). The number of deposited bacterial cells was determined for each image by comparing the changes between successive images. Bacterial cell deposition experiments in the RSPF system were conducted over a range of ionic strength conditions (10–300 mM KCl) with a cell concentration of  $10^7$ – $10^8$  cells/mL. The influent cell concentration for each deposition run was determined directly by visualizing cells in a counting chamber (Buerker-Tuerk chamber, Marienfeld Laboratory Glassware, Lauda-Königshofen, Germany). A flow rate of 5 mL/min, corresponding to a particle Peclet number (30) of 2.4, was selected to be comparable to the particle Peclet number estimated for the packed column.

## Results and Discussion

**Electrokinetic Potentials of Bacterial Cells and Collector Surfaces.** The influence of ionic strength on the zeta potentials of the bacteria and the quartz grains is presented in Figure 1. As shown, the bacteria and quartz grains are negatively charged at the pH of the experiments (5.6–5.8). For all surfaces, the zeta potential becomes less negative with increasing ionic strength due to compression of the electrostatic double layer. These zeta potential values are used later to calculate the DLVO interaction energies between the bacterial cells and the quartz grains (Table 1) to elucidate the bacterial adhesion mechanisms.

**Packed-Bed Transport of Bacterial Cells.** The adhesion and transport of *E. coli* D21g was systematically examined in saturated, packed beds of highly cleaned quartz grains. Typical breakthrough curves demonstrating the influence of ionic strength on transport are presented in Figure 2. In this figure, the normalized effluent concentration is plotted against the number of pore volumes passed through the column. Initially, the column effluent is free of bacterial cells. After approximately 1 pore volume, the injected bacteria cells break through the packed bed and are detected in the effluent. The influent is switched to a bacteria-free solution after

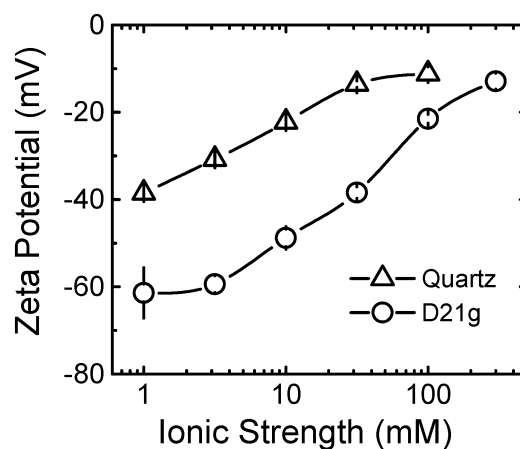


FIGURE 1. Zeta potentials of D21g bacterial cells and quartz grains as a function of ionic strength at unadjusted pH of 5.6–5.8. Error bars represent the standard error.

TABLE 1. Electrokinetic Properties of Bacteria and Quartz Sand as well as Calculated DLVO Interaction Parameters

ionic strength (mM)	zeta potential (mV)		energy barrier (kT)	secondary minimum depth (kT)	secondary minimum separation (nm)
	D21g	quartz sand			
1	-61.4	-38.5	2250	0.092	120
3.2	-59.4	-30.8	1440	0.39	57
10	-48.8	-22.2	650	1.8	25
31.6	-38.4	-13.6	140	8.1	10
100	-21.5	-11.6	NB <sup>a</sup>	NB <sup>a</sup>	NB <sup>a</sup>
300	-12.9	ND <sup>b</sup>	ND <sup>b</sup>	ND <sup>b</sup>	ND <sup>b</sup>

<sup>a</sup> No calculated barrier to deposition. <sup>b</sup> Not determined.

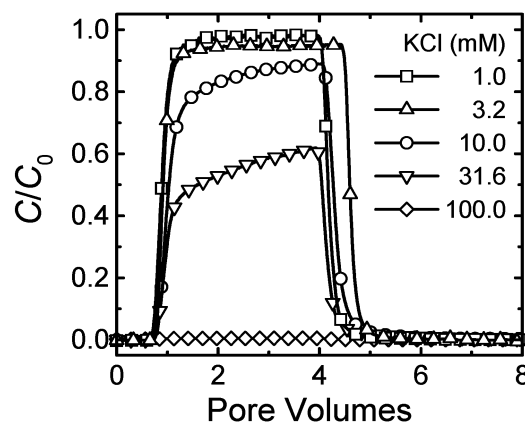


FIGURE 2. Normalized effluent concentration of D21g plotted against the number of pore volumes pumped through the packed bed for different pore fluid ionic strengths. For clarity, every 40th data point is plotted. Experimental conditions are indicated in Table 2 (first experiment for each ionic strength is plotted here). Other experimental parameters were approach velocity = 0.021 cm/s, porosity = 0.43, mean grain diameter = 205  $\mu$ m, and pH = 5.6–5.8.

approximately 4 pore volumes, and the concentration of bacteria in the effluent decreases.

In general, an increase in the ionic strength of the pore fluid results in increased deposition of the bacteria onto the quartz grains. For example, at the lowest ionic strength examined (1 mM), the normalized initial bacterial cell breakthrough concentration (at about pore volume 2) shown in Figure 2 is 0.97. As the ionic strength of the pore fluid is increased, bacterial retention in the column increases, and the normalized initial breakthrough concentration declines, from 0.94 at 3.2 mM, and 0.83 at 10 mM, to 0.52 at 31.6 mM.

**TABLE 2. Physical and Calculated Parameters for Packed-Bed Column Experiments**

ionic strength (mM)	column length, $L$ (cm)	$C_0$ (cells/mL)	$C/C_0^a$	$k_d$ ( $s^{-1}$ )	fraction eluted
<b>Unfavorable Deposition Experiments</b>					
1	13.6	$9.3 \times 10^7$	0.97	$1.1 \times 10^{-4}$	— <sup>b</sup>
	14.2	$8.3 \times 10^7$	0.99	$2.9 \times 10^{-5}$	—
	14.0	$1.1 \times 10^8$	0.95	$1.7 \times 10^{-4}$	—
3.2	22.5	$3.2 \times 10^7$	0.97	$8.1 \times 10^{-5}$	—
	12.2	$6.0 \times 10^7$	0.94	$2.4 \times 10^{-4}$	—
	11.9	$9.1 \times 10^7$	0.96	$1.5 \times 10^{-4}$	—
10	11.9	$3.7 \times 10^7$	0.97	$1.4 \times 10^{-4}$	—
	11.7	$5.8 \times 10^7$	0.96	$1.8 \times 10^{-4}$	—
	13.6	$2.5 \times 10^7$	0.83	$6.7 \times 10^{-4}$	—
14.1	14.1	$1.0 \times 10^8$	0.87	$5.1 \times 10^{-4}$	—
	14.2	$7.9 \times 10^7$	0.90	$3.7 \times 10^{-4}$	—
	9.2	$8.3 \times 10^6$	0.93	$4.1 \times 10^{-4}$	0.38
31.6	9.4	$1.1 \times 10^7$	0.89	$6.3 \times 10^{-4}$	0.53
	14.1	$1.0 \times 10^8$	0.52	$2.3 \times 10^{-3}$	—
	14.5	$6.2 \times 10^6$	0.41	$3.0 \times 10^{-3}$	—
100	13.8	$1.0 \times 10^8$	0.68	$1.4 \times 10^{-3}$	—
	13.6	$2.0 \times 10^6$	0.48	$2.7 \times 10^{-3}$	—
	8.9	$9.1 \times 10^6$	0.66	$2.3 \times 10^{-3}$	0.77
300	9.1	$8.2 \times 10^6$	0.60	$2.8 \times 10^{-3}$	0.76
	9.2	$1.3 \times 10^7$	0.71	$1.8 \times 10^{-3}$	0.78
	14.2	$8.4 \times 10^7$	0.0048	$1.9 \times 10^{-2}$	—
10	13.5	$9.8 \times 10^7$	0.0030	$2.1 \times 10^{-2}$	—
	13.7	$1.1 \times 10^8$	0.012	$1.6 \times 10^{-2}$	—
	7.3	$1.8 \times 10^7$	0.064	$1.9 \times 10^{-2}$	0.50
300	7.3	$7.1 \times 10^6$	0.11	$1.5 \times 10^{-2}$	0.85
	13.5	$1.8 \times 10^7$	0.0095	$3.1 \times 10^{-2}$	0.54
<b>Favorable Deposition Experiments</b>					
10	1.6	$9.3 \times 10^6$	0.31	$3.6 \times 10^{-2}$	<0.01
	3.4	$1.0 \times 10^8$	0.11	$3.4 \times 10^{-2}$	<0.01

<sup>a</sup> Determined by averaging over pore volumes 1.8–2, as described in the text. <sup>b</sup> Elution pulse (0.1 mM KCl) not applied to column.

At the highest ionic strength shown, 100 mM, the normalized initial breakthrough concentration was 0.0048. Because of possible differences in surface properties between individual cultures of D21g, transport experiments were generally repeated between four and seven times at each ionic strength (a single experiment was conducted at 300 mM KCl). Relevant experimental parameters of all experiments are presented in Table 2.

To quantitatively compare the experiments, the deposition rate coefficient  $k_d$  was determined for each transport experiment presented in Table 2 using (31, 32):

$$k_d = -\frac{U}{fL} \ln\left(\frac{C}{C_0}\right) \quad (1)$$

where  $C/C_0$  is the normalized breakthrough concentration,  $U$  is the approach (superficial) fluid velocity,  $f$  is the packed-bed porosity, and  $L$  is the length of the packed bed. The deposition rate coefficient is directly related to the single collector removal efficiency,  $\eta$ , via (32, 33):

$$k_d = \frac{3}{2} \frac{(1-f)}{fd_c} U\eta \quad (2)$$

where  $d_c$  is the collector diameter. As illustrated in Figure 2, in some experiments the normalized cell concentration did not achieve a steady-state concentration after the initial dispersive region of breakthrough. Rather, the concentration increased slowly with time indicating either simultaneous bacterial release or blocking by previously deposited bacterial cells. Consequently, the initial clean bed  $C/C_0$  was determined

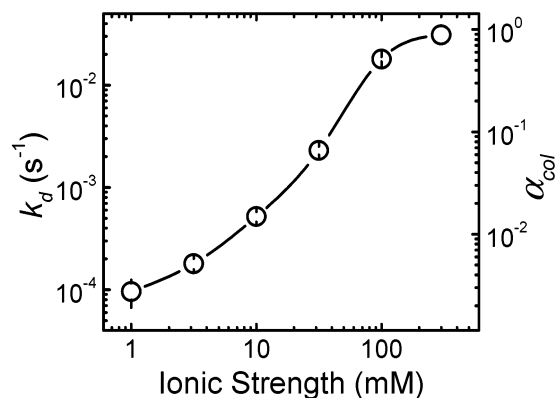


**FIGURE 3. Influence of ionic strength on the deposition rate coefficient, ( $k_d$ ) and the corresponding attachment efficiency, ( $\alpha_{col}$ ) of D21g in the quartz packed column. Each data point represents the average value determined from all experiments conducted at a given ionic strength. Error bars represent the standard error. Experimental conditions are given in Table 2 and Figure 2.**

for each experiment by averaging the normalized breakthrough concentrations measured between pore volumes 1.8 and 2.

The attachment efficiency for the packed-bed column,  $\alpha_{col}$ , can be determined for each experiment by normalizing  $k_d$  by the experimentally determined deposition rate coefficient under favorable electrostatic conditions ( $k_{d,fav}$ ) (31):

$$\alpha_{col} = \frac{k_d}{k_{d,fav}} \quad (3)$$

Favorable (i.e., nonrepulsive) electrostatic conditions were achieved by packing a column with quartz grains that had been surface-modified with aminosilane, which imparts a net positive zeta potential. From two experiments conducted with silanized grains, an average value of the favorable deposition rate,  $k_{d,fav} = 3.5 \times 10^{-2} s^{-1}$ , was determined.

The influence of ionic strength on the deposition rate coefficient  $k_d$  and the corresponding attachment efficiency  $\alpha_{col}$  is depicted in Figure 3. An increase in solution ionic strength from 1 to 300 mM results in an increase in average  $k_d$  from  $9.6 \times 10^{-5}$  to  $3.1 \times 10^{-2} s^{-1}$  and a corresponding increase in  $\alpha_{col}$  from  $2.7 \times 10^{-3}$  to 0.89. These results are in qualitative agreement with DLVO theory (30). In particular, an increase in ionic strength reduces the electrostatic double layer repulsive forces and hence the rate of bacterial deposition increases. This effect is discussed in more detail in the following section.

**Interpretation Using DLVO Theory—Interaction Energy Profiles.** Under all solution conditions analyzed, both the bacterial cells and the quartz grains have a net negative zeta potential, and repulsive electrostatic interactions should inhibit cell deposition. However, a clear trend of increasing deposition with increasing ionic strength is observed (Figure 3). To gain insight into the mechanism responsible for deposition, DLVO theory is used to calculate the total interaction energy as a bacterial cell approaches a quartz grain. The total interaction energy, namely, the sum of attractive van der Waals and repulsive electrostatic interactions, was calculated by modeling the bacteria-quartz grain system with a sphere-plate interaction.

Repulsive electrostatic double layer interaction energies were calculated using the Hogg et al. (34) expression:

$$\Phi_{EDL} = \pi\epsilon_0\epsilon_r a_p \left\{ 2\psi_p\psi_c \ln\left[\frac{1 + \exp(-\kappa h)}{1 - \exp(-\kappa h)}\right] + (\psi_p^2 + \psi_c^2) \ln[1 - \exp(-2\kappa h)] \right\} \quad (4)$$

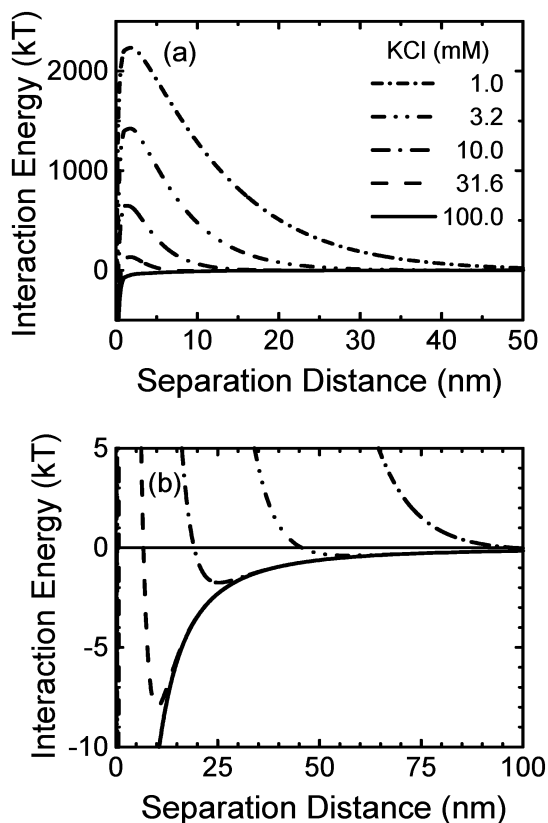


FIGURE 4. (a) Calculated DLVO interaction energy as a function of separation distance and ionic strength. Identical data are replotted in panel (b) to highlight the secondary energy minimum. Interaction energies were calculated from the experimentally determined zeta potentials (Table 1) for a Hamaker constant of  $6.5 \times 10^{-21}$  J and an equivalent bacterial cell radius of  $0.87 \mu\text{m}$ .

where  $\epsilon_0$  is the dielectric permittivity in a vacuum,  $\epsilon_r$  is the relative dielectric permittivity of water,  $a_p$  is the bacterial radius,  $\kappa$  is the inverse Debye length,  $h$  is the separation distance between the bacterium and the collector surface, and  $\psi_p$  and  $\psi_c$  are the surface potentials of the bacterial cell and quartz collector, respectively. Because the bacteria are rod shaped, the equivalent spherical radius of a spheroid having the same average major and minor axes as the bacteria was assumed (i.e.,  $a_p = 0.87 \mu\text{m}$ ). Additionally, the measured zeta potentials of both the bacteria and the collector (Table 1) were used in place of the respective surface potentials.

The retarded van der Waals attractive interaction energy was calculated from (35, 36):

$$\Phi_{\text{VDW}} = -\frac{Aa_p}{6h} \left[ 1 + \frac{14h}{\lambda} \right]^{-1} \quad (5)$$

where  $A$  is the Hamaker constant of the interacting media (bacteria–water–quartz), and  $\lambda$  is the characteristic wavelength of the dielectric (assumed to be 100 nm). A value of  $6.5 \times 10^{-21}$  J was used for the Hamaker constant (15, 17).

The variation of the DLVO interaction energy with separation distance at different ionic strengths is illustrated in Figure 4a. As shown, for solutions with ionic strength less than or equal to 31.6 mM, calculations predict the presence of a substantial repulsive energy barrier to bacterial deposition ranging from 140 kT at 31.6 mM to over 2000 kT at 1 mM (see also Table 1). Because surface chemical heterogeneities are probably negligible for the highly pure quartz collectors, the huge energy barriers suggest that it is unlikely that the bacterial cells will deposit in the primary energy minimum at the quartz surface.

**Interpretation Using DLVO Theory—Role of the Secondary Minimum.** The van der Waals and electrostatic double layer interactions have different dependencies with respect to separation distance (power-law and exponential, respectively). Consequently, calculations of the total interaction energy predict the presence of a secondary energy minimum at a greater separation distance than that of the energy barrier. The DLVO profiles are replotted in Figure 4b to emphasize the magnitude of this secondary energy minimum. Bacteria approaching a quartz grain would first experience an attractive force before encountering the significant repulsive energy barrier. Cells unable to overcome the energy barrier could remain associated with the quartz grain within the secondary energy minimum unless they had sufficient energy to escape (37). The magnitude of the secondary energy minimum increases with ionic strength. In particular, the depth of secondary minima ranges from 0.09 kT at 1 mM to 8.1 kT at 31.6 mM, with corresponding separation distances of 120–10 nm, respectively, as listed in Table 1. Because the thermal energy of a bacterium is on the order of 0.5 kT, the secondary minima depths shown in Table 1 for ionic strengths greater than 10 mM should be sufficient to retain bacterial cells in the packed-bed column (37).

The secondary minimum depths discussed previously were calculated by assuming that the electrostatic component of the DLVO interactions followed the Hogg et al. expression for interaction at constant surface potentials (34). Other models for calculating electrostatic interactions include assuming a constant surface charge or by compromising between the two approaches and relaxing the assumption of constant charge or potential, the so-called linear superposition approximation (LSA) (30). The three models of electrostatic interactions are similar for separation distances greater than about 5 nm; however, at closer distances they can exhibit markedly different behavior. At 100 mM, for example, the constant surface potential model calculations shown in Figure 4b predict no energy barrier to deposition. However, for the same ionic strength, if a constant surface charge were assumed, the DLVO calculations would indicate the presence of an 8 kT energy barrier and a very deep secondary energy minimum (33 kT). Consequently, predictions of the presence or absence of an energy barrier and a secondary energy minimum at moderate to high ionic strengths are strongly dependent on the model chosen for the calculation of electrostatic double layer interaction.

The depth of the secondary energy minimum as well as the height of the energy barrier depend on a number of factors, including the surface potentials of both the bacterial cell and the quartz grain ( $\psi_p$  and  $\psi_c$ , respectively), the range of the electrostatic double layer interactions (characterized by the inverse Debye length,  $\kappa$ ), and the van der Waals interactions between the two surfaces (characterized by the Hamaker constant,  $A$ ). Elimelech (38) formulated a dimensionless parameter that incorporates these factors and characterizes the interaction energy for unfavorable deposition:

$$N_{\text{DLVO}} = \frac{\kappa A}{\epsilon_0 \epsilon_r \psi_p \psi_c} \quad (6)$$

where all terms have been defined earlier.

If the zeta potentials of both the cells and the quartz grains are used instead of the surface potentials,  $N_{\text{DLVO}}$  can be calculated for each ionic strength condition studied. The relationship between  $N_{\text{DLVO}}$  and the bacterial cell attachment efficiency,  $\alpha_{\text{col}}$ , is shown in Figure 5. The correlation between  $\alpha_{\text{col}}$  and  $N_{\text{DLVO}}$  fits a power law having a slope near unity (exponent = 1.1,  $r^2 = 0.98$ ). The excellent agreement between the dimensionless  $N_{\text{DLVO}}$  parameter and  $\alpha_{\text{col}}$  strongly suggests that electrostatic and van der Waals components are the

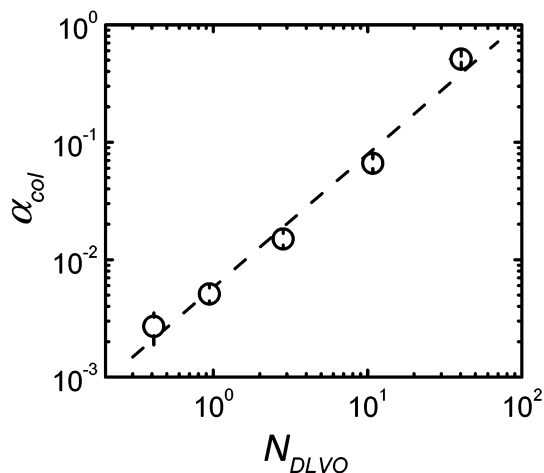


FIGURE 5. Dependence of the experimentally determined average attachment efficiencies and the dimensionless DLVO number,  $N_{DLVO}$ , calculated at each ionic strength (excluding 300 mM, as the zeta potential of the quartz was not determined). Error bars indicate the standard error. Dashed line indicates best-fit power-law, which has an exponent of 1.1. Attachment efficiencies are replotted from Figure 3.  $N_{DLVO}$  was calculated from the experimentally determined zeta potentials (Table 1), for a Hamaker constant of  $6.5 \times 10^{-21}$  J.

dominant forces affecting the bacterial cell–quartz grain interactions.

As indicated in Figure 4a, sizable energy barriers exist to inhibit bacterial deposition at most ionic strengths examined. However, experimental evidence shows a clear trend of the deposition rate increasing with ionic strength. This ionic strength dependence of  $k_d$  parallels the increase in calculated secondary energy minimum depths with increasing ionic strength. It is therefore possible that bacterial deposition is not occurring in the primary energy minimum at the grain surface but predominantly in secondary energy minima some distance from the grain surface. To test this hypothesis, two sets of supporting experiments were conducted. In the first,

the ionic strength of the pore fluid was adjusted to examine the release of previously deposited cells, while in the second, a radial stagnation point flow system was used to examine the deposition behavior of individual cells.

**Reversibility of Deposited Cells—Evidence for Deposition in Secondary Minima.** To investigate whether the bacterial cells retained in the packed bed during a transport experiment were indeed deposited in secondary energy minima, a number of release experiments were conducted (Table 2). In these experiments, bacteria were initially deposited at moderate to high ionic strengths (10–300 mM KCl) and released by application of a low ionic strength solution. A 0.1 mM KCl solution was selected as the background electrolyte because it has such a sufficiently low ionic strength that it should eliminate the presence of a secondary energy minimum, thus releasing any bacteria that may have previously deposited there.

An example breakthrough curve demonstrating bacterial elution is presented in Figure 6. As can be seen, a pulse of released bacteria is eluted from the column beginning 1 pore volume after the 0.1 mM KCl solution was applied. By numerically integrating the breakthrough curve, it is possible to calculate the amount of bacterial cells adhered to the quartz grains prior to the injection of the 0.1 mM KCl solution and the amount of cells released in the elution pulse. From these calculations, the fraction of deposited cells that was eluted by the change in ionic strength of the pore fluid can be determined. As shown in Table 2, a significant fraction of the deposited bacterial cells are eluted from the column when the low ionic strength solution was introduced, ranging from an average of 0.45 when the cells were deposited in 10 mM to  $>0.68$  when the cells were deposited at higher ionic strengths. Release experiments were not conducted at ionic strengths lower than 10 mM, as the breakthrough concentrations in the deposition portion of the experiment were near unity ( $C/C_0 > 0.94$  in all cases), indicating that a small amount of cells were deposited in the column.

The release of the majority of deposited cells suggests that the bacteria were not irreversibly attached to the quartz grain in a primary minimum but initially deposited within

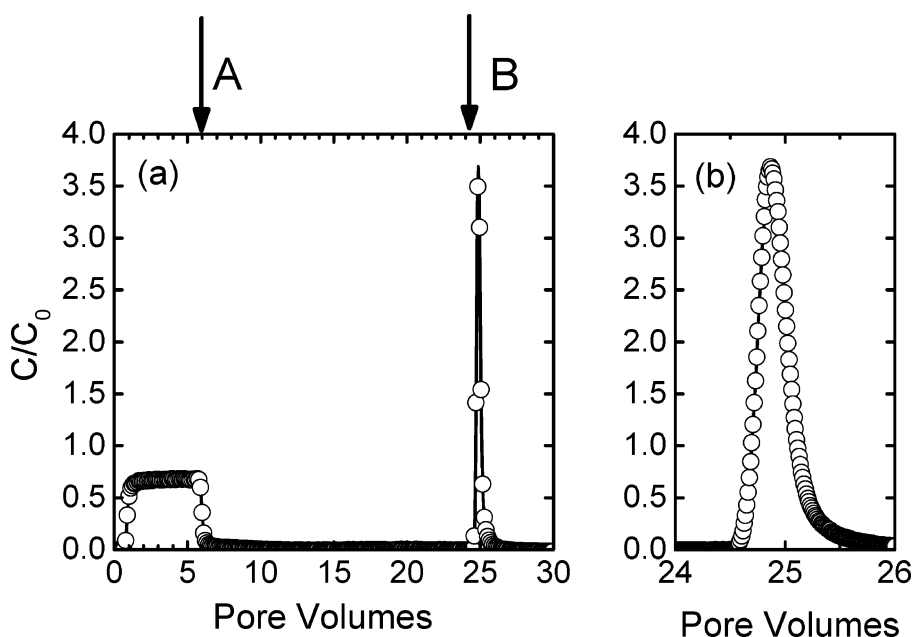


FIGURE 6. Example of bacterial release induced by ionic strength reduction of the pore fluid. Bacteria are initially applied to the column in a 31.6 mM KCl solution. Arrows indicate the application of 31.6 mM bacteria-free solution (A) and 0.1 mM bacteria-free solution (B). The pulse of released bacteria is coincident with low ionic strength pore fluid (B). Relevant experimental conditions are in Figure 2 and Table 2 (plotted here is the first elution experiment listed for 31.6 mM KCl). Panel (a) shows complete breakthrough curve (with every 10th data point shown for clarity) and panel (b) focuses on the release portion (PV 24–26) with every data point shown.

secondary energy minima. Release of deposited cells occurred in all repulsive electrostatic cases examined but was less than 100% of the deposited amount. Possible explanations for partial release include (a) physical straining, (b) surface roughness, (c) subsequent deposition of released cells, and (d) primary minimum deposition. Each of these is discussed next.

**(a) Physical Straining.** Straining occurs when the particle size is physically larger than the pore space, leading to removal from the pore fluid by mechanical means. While traditionally straining has been considered an important removal mechanism when the particle–collector size ratio is greater than 0.05 (39), Bradford et al. (40) recently proposed straining as a feasible particle capture mechanism for systems where the ratio of particle size to the average grain size is much smaller. Although the size ratio (based on average grain size) for our bacteria–quartz sand system is relatively small, on the order of 0.009, straining may still be possible because of the irregular shape of the quartz grains. However, given the low degree of removal observed at the lowest ionic strength ( $C/C_0$  between 0.95 and 0.99 at 1 mM, as shown in Table 2), it is unlikely that straining can account for the retained bacteria during the elution step.

**(b) Surface Roughness.** The quartz grains used in this study are quite angular, with asperities comparable in size to the bacteria visible under a scanning electron microscope (41). Surface roughness has been documented to influence the deposition behavior of colloidal particles (42, 43). However, the influence of roughness on release is uncertain. Interaction energy profiles are strongly affected by surface features (43, 44), and the irregular surface of the quartz grains likely gives rise to a complex distribution of interaction energies and deposition mechanisms. Heterogeneity in the interaction energy profiles could potentially lead to particles irreversibly attached to the quartz surface.

**(c) Release and Subsequent Deposition.** Another explanation for the less than complete elution of bacteria is subsequent redeposition of bacteria that were released. However, the near complete bacterial cell breakthrough in a 1 mM solution (Table 2 and Figure 2) suggests otherwise. The repulsive electrostatic interactions are greater in the 0.1 mM elution solution, which should greatly reduce the potential for released cells to deposit in the packed bed.

**(d) Primary Minimum Deposition.** Despite predictions of substantial energy barriers at most ionic strengths examined, charge heterogeneity of the bacterial cells, both at the local (cellular) scale (45–47) and within the bacterial population as a whole (16, 48), could give rise to a range of interaction energy profiles. Certain bacterial cells may thus experience less repulsive or even attractive interaction energies upon close approach, which may lead to primary minimum deposition. It is possible that these bacterial cells are still retained on the quartz grain after the ionic strength has been lowered and the repulsive electrostatic interactions are increased.

Conversely, at solution ionic strength  $\geq 100$  mM KCl, the interaction energy calculations indicate no energy barrier to deposition, suggesting that cells may be depositing in a primary minimum. However, cells are observed to release when the ionic strength is lowered. As mentioned previously, heterogeneity at various scales likely exists, and the calculated interaction energy at 100 mM may not accurately reflect the interactions between individual bacteria and a quartz grain. A portion of the bacterial population may actually be depositing in secondary energy minima, and thus, released upon ionic strength perturbation. Furthermore, as discussed earlier, the choice of model used to determine electrostatic interaction energies can dramatically affect predictions of presence of energy barrier and secondary energy minima. It is possible that the constant potential interaction model used

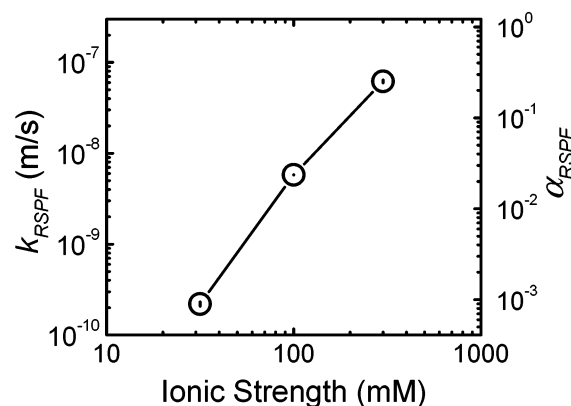


FIGURE 7. Bacterial deposition kinetics for the radial stagnation point flow system expressed as bacterial deposition rate coefficient,  $k_{RSFP}$ , and attachment efficiency,  $\alpha_{RSFP}$ , versus ionic strength. The average number of deposited cells at 10 mM KCl was less than 1 over a 20 min period; hence,  $k_{RSFP}$  and  $\alpha_{RSFP}$  values are not determined. Error bars indicate the standard error.

in this study does not fully capture the electrostatic double layer interactions between the bacteria and the quartz and may erroneously predict the absence of energy barrier and secondary minimum at higher ionic strengths. Last, invoking short-range repulsive Born potential or a distance of closest approach, which creates a finite and relatively shallow primary minimum, may explain ionic strength perturbation induced release of bacteria that were initially predicted to be deposited in a primary minimum (49).

**Deposition in Radial Stagnation Point Flow System.** To further investigate whether initial bacterial deposition is occurring in secondary energy minima, a radial stagnation point flow (RSPF) system was used to examine the microscopic aspects of bacterial transport and deposition by directly visualizing the attachment of bacterial cells to a quartz cover slip. Specifically, the RSPF system simulates the hydrodynamics and deposition behavior at the forward stagnation point of a spherical collector surface. A highly cleaned quartz cover slip was used as the collector surface to mimic as close as possible the DLVO interactions within the packed-bed column experiments. The hydrodynamic conditions in the RSPF and packed-bed column were comparable, with the particle Peclet numbers (defined on page 75 of ref 30) equal to 2.4 for the RSPF system and 4.5 for the packed column based on a mean grain diameter ( $d_{50}$ ) of 205  $\mu\text{m}$ .

Bacterial deposition onto the cover slip was quantified by determining a bacterial transfer rate coefficient,  $k_{RSFP}$ :

$$k_{RSFP} = \frac{J}{C_0} \quad (7)$$

where  $J$  is the bacterial deposition flux to the cover slip. The deposition flux was determined by normalizing the observed deposition rate of bacteria on the cover slip (i.e., the initial slope of the number of deposited bacteria vs time curve) by the microscope viewing area ( $210 \times 165 \mu\text{m}$ ). As with the packed-bed experiments, the attachment efficiency in the RSPF system,  $\alpha_{RSFP}$ , was calculated by normalizing the bacterial transfer rate coefficient at each ionic strength by the transfer rate coefficient determined under favorable (nonrepulsive) electrostatic conditions (using an amino-silanized cover slip). The resulting average bacterial transfer rate coefficient under favorable conditions is  $k_{RSFP, fav} = 2.45 \times 10^{-7}$  m/s.

The influence of ionic strength on  $k_{RSFP}$  and  $\alpha_{RSFP}$  is shown in Figure 7. Similar to the column experiments, bacterial adhesion to the collector surface increased with increasing

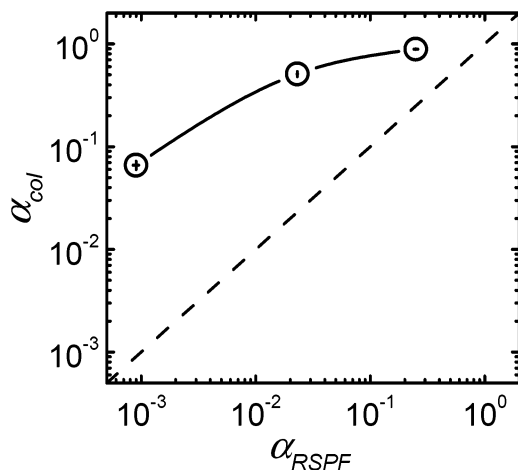


FIGURE 8. Correlation between attachment efficiencies in the packed-bed column ( $\alpha_{col}$ ) and RSPF ( $\alpha_{RSPF}$ ) systems. Data are replotted from Figures 3 and 7 for ionic strengths where values of the attachment efficiency could be determined. Dashed line indicates a perfect correlation between RSPF and packed-bed column attachment efficiencies. Error bars indicate the standard error.

ionic strength. However, while this trend is in general agreement with observations from the packed-bed column experiments, the values of  $\alpha_{RSPF}$  are much smaller than  $\alpha_{col}$  for identical ionic strengths. Most conspicuous is that experiments conducted at 10 mM KCl resulted in negligible deposition over the duration of the deposition experiment (i.e., average number of cells depositing over 20 min was less than 1 in four replicate experiments with cell concentrations as high as  $1.5 \times 10^8$  cells/mL). By contrast, at 10 mM KCl, an attachment efficiency of 0.015 was measured in the packed-bed experiments.

This striking difference in attachment efficiencies can be understood by examining the difference in the hydrodynamics between the RSPF and the packed-bed column systems. Bacteria entrained in a secondary energy minimum experience hydrodynamic forces due to the radial component of flow along the collector surface (50). In the RSPF system, these bacteria would be swept away from the stagnation point region and the microscope's field of view by the radial flow parallel to the surface. In contrast, cells that deposit in secondary energy minima on a collector grain will be transported along the grain surface and accumulate in either the rear stagnation point (51) or other regions of stagnant flow on the collector grain created by the grain surface irregularities. Thus, in the RSPF system, only cells that are irreversibly deposited in a primary energy minimum are enumerated, while in the packed-bed column, all cells that are retained—either deposited in a primary energy minimum on the grain surface or held in a secondary energy minimum—are accounted for. As stated earlier, bacterial deposition in primary minimum in both systems is attributed to local charge heterogeneities on bacterial cells as well as heterogeneity in the bacterial cell population. Local charge heterogeneity on the quartz collector may also result in primary minimum deposition, but its impact is expected to be much less important than cell heterogeneity, due to the high purity of the quartz collectors and the extensive cleaning method.

The salient difference between the two experimental systems is depicted in Figure 8, where the attachment efficiency for the column experiments,  $\alpha_{col}$ , is plotted against the attachment efficiency for the RSPF system,  $\alpha_{RSPF}$ . In this graph, if the measured attachment efficiencies were identical in both systems, the data would fall along the dashed line of unity slope. However, as shown in the figure,  $\alpha_{col}$  is much greater than  $\alpha_{RSPF}$  for all ionic strengths. As discussed

previously, this discrepancy arises from enumeration of only those cells deposited in a primary energy minimum in the RSPF system. At the lowest ionic strength for which  $\alpha_{RSPF}$  could be measured (31.6 mM), an almost 2 order of magnitude discrepancy was observed in the attachment efficiencies between the two experimental systems; however, at the highest ionic strength examined (300 mM), the attachment efficiencies differed by a factor of approximately 4. This suggests that decreased electrostatic repulsive forces arising from the increase in solution ionic strength leads to greater primary minimum deposition and closer agreement between the measured attachment efficiencies in the two systems.

The absence of deposition at moderate (10 mM) and lower ionic strengths in the RSPF system, the order of magnitude difference between the attachment efficiencies of D21g in the RSPF system and the packed-bed experiments, and the significant release of bacterial cells in column experiments following reduction in ionic strength imply that the majority of bacteria in our column experiments are weakly attached in secondary energy minima. We therefore propose that the secondary minimum plays an important role in bacterial transport and deposition in granular porous media.

### Acknowledgments

This work was supported by the National Science Foundation, Collaborative Research Activities in Environmental Molecular Sciences (Grant CHE-0089156), the Yale Institute for Biospheric Studies, and the National Water Research Institute. We would also like to acknowledge Professor H. P. Spink (Leiden University, The Netherlands) for use of the EGFP plasmid.

### Note Added after ASAP Posting

This paper was released ASAP on 02/10/2004 with incorrect axis labels in Figure 6 (data unchanged). The correct version was posted on 02/13/2004.

### Literature Cited

- (1) Gross, M. J.; Logan, B. E. *Appl. Environ. Microbiol.* **1995**, *61*, 1750–1756.
- (2) Rittmann, B. E. *Civil Eng.* **1996**, *66*, 50–52.
- (3) Gannon, J. T.; Manilal, V. B.; Alexander, M. *Appl. Environ. Microbiol.* **1991**, *57*, 190–193.
- (4) van Loosdrecht, M. C. M.; Lyklema, J.; Norde, W.; Schraa, G.; Zehnder, A. J. B. *Appl. Environ. Microbiol.* **1987**, *53*, 1893–1897.
- (5) Schafer, A.; Harms, H.; Zehnder, A. J. B. *Environ. Sci. Technol.* **1998**, *32*, 3704–3712.
- (6) van Loosdrecht, M. C. M.; Lyklema, J.; Norde, W.; Schraa, G.; Zehnder, A. J. B. *Appl. Environ. Microbiol.* **1987**, *53*, 1898–1901.
- (7) Vigeant, M. A. S.; Ford, R. M.; Wagner, M.; Tamm, L. K. *Appl. Environ. Microbiol.* **2002**, *68*, 2794–2801.
- (8) Camesano, T. A.; Logan, B. E. *Environ. Sci. Technol.* **1998**, *32*, 1699–1708.
- (9) Gross, M.; Cramton, S. E.; Gotz, F.; Peschel, A. *Infect. Immun.* **2001**, *69*, 3423–3426.
- (10) Burks, G. A.; Velegol, S. B.; Paramonova, E.; Lindenmuth, B. E.; Feick, J. D.; Logan, B. E. *Langmuir* **2003**, *19*, 2366–2371.
- (11) Smets, B. F.; Grasso, D.; Engwall, M. A.; Machinist, B. J. *Colloid Surf. B* **1999**, *14*, 121–139.
- (12) Jucker, B. A.; Zehnder, A. J. B.; Harms, H. *Environ. Sci. Technol.* **1998**, *32*, 2909–2915.
- (13) Poortinga, A. T.; Bos, R.; Norde, W.; Busscher, H. J. *Surf. Sci. Rep.* **2002**, *47*, 3–32.
- (14) Poortinga, A. T.; Bos, R.; Busscher, H. J. *Langmuir* **2001**, *17*, 2851–2856.
- (15) Simoni, S. F.; Bosma, T. N. P.; Harms, H.; Zehnder, A. J. B. *Environ. Sci. Technol.* **2000**, *34*, 1011–1017.
- (16) Baygents, J. C.; Glynn, J. R.; Albinger, O.; Biesemeyer, B. K.; Ogden, K. L.; Arnold, R. G. *Environ. Sci. Technol.* **1998**, *32*, 1596–1603.
- (17) Truesdail, S. E.; Lukasik, J.; Farrah, S. R.; Shah, D. O.; Dickinson, R. B. *J. Colloid Interface Sci.* **1998**, *203*, 369–378.
- (18) Hermansson, M. *Colloid Surf. B* **1999**, *14*, 105–119.
- (19) Rijnaarts, H. H. M.; Norde, W.; Lyklema, J.; Zehnder, A. J. B. *Colloid Surf. B* **1995**, *4*, 191–197.

- (20) Azeredo, J.; Visser, J.; Oliveira, R. *Colloid Surf. B* **1999**, *14*, 141–148.
- (21) Meinders, J. M.; van der Mei, H. C.; Busscher, H. J. *J. Colloid Interface Sci.* **1995**, *176*, 329–341.
- (22) Litton, G. M.; Olson, T. M. *Environ. Sci. Technol.* **1993**, *27*, 185–193.
- (23) Stuurman, N.; Bras, C. P.; Schlaman, H. R. M.; Wijffes, A. H. M.; Bloemberg, G.; Spaink, H. P. *Mol. Plant-Microbe Interact.* **2000**, *13*, 1163–1169.
- (24) Sambrook, J.; Fritsch, E. F.; Maniatis, T. *Molecular Cloning, A Laboratory Manual*, 2nd ed.; Cold Spring Harbor Laboratory Press: Cold Spring Harbor, New York, 1989; Vol. 3.
- (25) Litton, G. M. Ph.D. Dissertation, University of California, Irvine, 1996.
- (26) Adamczyk, Z.; Siwek, B.; Zembala, M.; Warszynski, P. *J. Colloid Interface Sci.* **1989**, *130*, 578–587.
- (27) Gomez-Suarez, C.; Pasma, J.; van der Borden, A. J.; Wingender, J.; Flemming, H. C.; Busscher, H. J.; van der Mei, H. C. *Microbiol-Sgm* **2002**, *148*, 1161–1169.
- (28) Ottewill, R. H.; Shaw, J. N. *J. Electroanal. Chem.* **1972**, *37*, 133.
- (29) Elimelech, M.; Nagai, M.; Ko, C. H.; Ryan, J. N. *Environ. Sci. Technol.* **2000**, *34*, 2143–2148.
- (30) Elimelech, M.; Gregory, J.; Jia, X.; Williams, R. A. *Particle Deposition and Aggregation-Measurement, Modeling and Simulation*; Butterworth-Heinemann: Woburn, MA, 1995.
- (31) Kretschmar, R.; Borkovec, M.; Grolimund, D.; Elimelech, M. *Advances in Agronomy* **1999**, *66*, 121–193.
- (32) Tufenkji, N.; Elimelech, M. *Environ. Sci. Technol.* **2004**, *38*, 529–536.
- (33) Grolimund, D.; Elimelech, M.; Borkovec, M.; Barmettler, K.; Kretschmar, R.; Sticher, H. *Environ. Sci. Technol.* **1998**, *32*, 3562–3569.
- (34) Hogg, R.; Healy, T. W.; Fuerstenau, D. W. T. *Faraday Soc.* **1966**, *62*, 1638–1651.
- (35) Elimelech, M.; O'Melia, C. R. *Langmuir* **1990**, *6*, 1153–1163.
- (36) Gregory, J. J. *Colloid Interface Sci.* **1981**, *83*, 138–145.
- (37) Hahn, M. W.; O'Melia, C. R. *Environ. Sci. Technol.* **2004**, *38*, 210–220.
- (38) Elimelech, M. *Water Res.* **1992**, *26*, 1–8.
- (39) Sakthivadivel, R. *Theory and mechanism of filtration of non-colloidal fines through a porous medium*; Rep. HEL 15-5; Hydraulic Engineering Lab., University of California: Berkeley, CA, 1966.
- (40) Bradford, S. A.; Simunek, J.; Bettahar, M.; Van Genuchten, M. T.; Yates, S. R. *Environ. Sci. Technol.* **2003**, *37*, 2242–2250.
- (41) Redman, J. A. Ph.D. Dissertation, University of California, Irvine, 2001.
- (42) Shellenberger, K.; Logan, B. E. *Environ. Sci. Technol.* **2002**, *36*, 184–189.
- (43) Bhattacharjee, S.; Ko, C. H.; Elimelech, M. *Langmuir* **1998**, *14*, 3365–3375.
- (44) Czarnecki, J.; Warszynski, P. *Colloid Surf.* **1987**, *22*, 207–214.
- (45) Jones, J. F.; Feick, J. D.; Imoudu, D.; Chukwumah, N.; Vigeant, M.; Velegol, D. *Appl. Environ. Microbiol.* **2003**, *69*, 6515–6519.
- (46) Sokolov, I.; Smith, D. S.; Henderson, G. S.; Gorby, Y. A.; Ferris, F. G. *Environ. Sci. Technol.* **2001**, *35*, 341–347.
- (47) Cox, J. S.; Smith, D. S.; Warren, L. A.; Ferris, F. G. *Environ. Sci. Technol.* **1999**, *33*, 4514–4521.
- (48) Dong, H. L. *J. Microbiol. Methods* **2002**, *51*, 83–93.
- (49) Ryan, J. N.; Gschwend, P. M. *J. Colloid Interface Sci.* **1994**, *165*, 536–536.
- (50) Adamczyk, Z.; Siwek, B.; Warszynski, P.; Musial, E. *J. Colloid Interface Sci.* **2001**, *242*, 14–24.
- (51) Spielman, L. A. *Annu. Rev. Fluid Mech.* **1977**, *9*, 297–319.

Received for review August 11, 2003. Revised manuscript received December 22, 2003. Accepted January 7, 2004.

ES034887L